Small patients, significant findings

Electrophysiological properties of Bachmann's bundle in pediatric patients

Dai, Lixia; Zhang, Can; Freriks, Anouk I.; Zheng, Jiahao; Linderhof, Manouk H.C.; van Schie, Mathijs S.; Yildirim, Vehpi; Knops, Paul; de Groot, Natasja M.S.; More Authors

DOI
10.1016/j.hrthm.2025.06.049

Publication date
2025

Document Version
Final published version

Published in
Heart Rhythm

Citation (APA)
Dai, L., Zhang, C., Freriks, A. I., Zheng, J., Linderhof, M. H. C., van Schie, M. S., Yildirim, V., Knops, P., de Groot, N. M. S., & More Authors (2025). Small patients, significant findings: Electrophysiological properties of Bachmann's bundle in pediatric patients. *Heart Rhythm*, *22*(11), 2766-2773. https://doi.org/10.1016/j.hrthm.2025.06.049

HeartRhythm

The Official Journal of the Heart Rhythm Society, The Cardiac Electrophysiology Society, and The Pediatric & Congenital Electrophysiology Society

Heart Rhythm Society SM

Check for updates

Small patients, significant findings: Electrophysiological properties of Bachmann's bundle in pediatric patients

Lixia Dai, MD,[1] Can Zhang, MD,[1] Anouk I. Freriks, MD,[1] Jiahao Zheng, MSc,[1] Manouk H.C. Linderhof, MD,[1] Hoang H. Nguyen, MD,[2] Mathijs S. van Schie, PhD,[1] Vehpi Yildirim, PhD,[1] Paul Knops, BSc,[1] Nawin Ramdat Misier, BSc,[1] Annemien E. van den Bosch, MD, PhD,[1] Wouter J. van Leeuwen, MD,[3] Pieter van de Woestijne, MD,[3] Jolanda Kluin, MD, PhD,[3] Yannick J.H.J. Taverne, MD, PhD,[3] Natasja M.S. de Groot, MD, PhD[1,4]

ABSTRACT

BACKGROUND Bachmann's bundle (BB) may potentially play a role in the earlier onset and faster progression of atrial fibrillation in adult patients with congenital heart disease (CHD). It is unknown whether electrophysiological alterations already exist at BB in *pediatric* patients with CHD and whether they are related to aging.

OBJECTIVE This study aimed to investigate BB electrophysiology in pediatric patients with CHD and assess the impact of age on BB electrophysiology.

METHODS BB mapping was conducted in 55 patients (0.2–17.5 years). Activation patterns, potential voltages, low-voltage areas (LVAs), potential morphology, and conduction disorders of BB were analyzed and correlated with age.

RESULTS Right-to-left activation across BB occurred in 96.4% of patients. Potential voltage was on average 7.2 ± 3.0 mV, and LVAs occurred in 85.4% of patients. Median local conduction velocity was 96.6 (72.9–121.0) cm/s, and conduction block occurred in 56.4% of patients. Most potentials were single and short-double potentials; long-double and fractionated potentials were recorded in 49.1% and 72.7% of patients, respectively. Age was weakly correlated with potential voltages ($r = 0.312$, $P = .020$) and moderately with local conduction velocity ($r = 0.439$, $P < .001$), but not with potential morphology or conduction block.

CONCLUSION In pediatric patients with CHD, BB already contains a considerable amount of conduction disorders, LVAs, and potentials with complex morphology. The prevalence of these early electrophysiological alterations is not age related and does not differ among the right, left, and middle parts of BB.

KEYWORDS Bachmann's bundle; Pediatric patients; Congenital heart disease; Age; Electrophysiology

(Heart Rhythm 2025;22:2766–2773)

Introduction

Bachmann's bundle (BB) is the bundle of muscle fibers that runs from the superior cavoatrial junction of the right atrium (RA) over the roof of the left atrium (LA) toward the LA appendage and is the preferential route for interatrial conduction.[1] In adult patients with coronary artery and/or valvular heart disease, aging, obesity, and long-term atrial volume overload are associated with conduction disorders across BB, even during sinus rhythm (SR).[2–5] In addition, the presence of conduction disorders and low-voltage potentials at BB are associated with the development of postoperative atrial fibrillation (AF).[6,7] Studies have also shown that patients with previous AF episodes have more conduction disorders,[7–9] decreased potential voltages,[8] and more

From the [1]Department of Cardiology, Erasmus Medical Center, Rotterdam, The Netherlands, [2]Department of Pediatrics, University of Texas Southwestern Medical Center, Dallas, Texas, [3]Department of Cardiothoracic Surgery, Erasmus Medical Center, Rotterdam, The Netherlands, and [4]Department of Microelectronics, Signal Processing Systems, Faculty of Electrical Engineering, Mathematics and Computer Sciences, Delft University of Technology, Delft, The Netherlands.

https://doi.org/10.1016/j.hrthm.2025.06.049

midentry activation[9] at BB than patients without a history of AF.

Patients with congenital heart disease (CHD) develop AF more frequently and at a younger age than the general population,[10] with a more rapid progression. This increased susceptibility to AF could be explained by a considerable amount of electropathology at BB. Indeed, Houck et al[2] reported that conduction disorders in adult patients with CHD during SR are most pronounced at BB. However, the structure and electrophysiological properties of the pediatric heart differ significantly from the adult heart,[11] hampering translation of BB mapping data from adult patients with CHD to children. Importantly, Kharbanda et al[3] recently showed that conduction disorders are already present at BB in 10 patients with CHD younger than 43 months. However, the extent of these abnormalities in pediatric BB and their relationship with age remain unclear. Therefore, this study aimed to characterize the electrophysiological properties of BB in a large cohort of pediatric patients with CHD up to 18 years old.

Methods

Study population

The study population consisted of 55 pediatric patients with CHD undergoing corrective surgery in the Erasmus Medical Center; none of these patients had previous cardiac surgery. Among all 188 pediatric patients with CHD included for epicardial mapping in the period between May 2020 and June 2024, 133 were excluded owing to the following: (1) unavailability of a small electrode to map during the early stages of this study, which particularly limited the inclusion of younger patients (<1 year); (2) BB could not be reached during surgery because the electrode could not be positioned at the correct location; or (3) low signal-to-noise ratio. Baseline characteristics and age distribution of the 133 excluded patients are presented in Supplemental Figure 1 and Supplemental Table 1.

This study was approved by the institutional medical ethical committee (MEC 2019-0543) and conducted according to the Declaration of Helsinki principles. A written informed consent was obtained from patients older than 16 years and parents of children younger than 16 years. Clinical characteristics of patients were retrieved from digital medical records.

Abbreviations

AF: atrial fibrillation

BB: Bachmann's bundle

CB: conduction block

CHD: congenital heart disease

FP: fractionated potential

LDP: long-double potential

LVA: low-voltage area

SDP: short-double potential

SP: single potential

SR: sinus rhythm

Epicardial mapping procedure

Epicardial high-resolution mapping of BB was performed before extracorporeal circulation, as previously described.[7] Depending on the age and cardiac size of the patients, a 96- (4 × 24) or 192-electrode (8 × 24) array (interelectrode distance 2.12 mm, electrode diameter 0.55 mm) was used for BB mapping. The array was positioned within the sinus transversus, behind the aorta with its tip against the LA appendage (Figure 1A). As demonstrated in Figure 1A, the mapping array was divided into 3 different equal parts to investigate differences in electrophysiological properties among the left (L_{BB}), middle (M_{BB}), and right (R_{BB}) parts of BB. Five seconds of SR was recorded, consisting of a surface electrocardiogram (ECG) lead, a calibration signal with an amplitude of 2 mV and a duration of 1000 ms, a bipolar reference electrogram (from a fixed RA appendage position), and all unipolar electrograms.

Data analysis

A custom-made software was used for the analysis of atrial potentials. As shown in Figure 1B, unipolar potentials were separated into 4 potential types based on their morphology, including (1) single potential (SP: 1 single deflection), (2) short-double potential (SDP: 2 deflections with a time interval <15 ms), (3) long-double potential (LDP: 2 deflections with a time interval ≥15 ms), and (4) fractionated potential (FP: ≥3 deflections). Color-coded activation maps were created by annotating the steepest negative slope of a unipolar potential as local activation time (LAT). All annotations were checked by 2 investigators. Potential voltage was defined as the peak-to-peak amplitude of the steepest negative deflection, and low-voltage areas (LVAs) were defined as the proportion of potential voltages of <1.0 mV among all potentials.[12] An epicardial breakthrough wave was defined as a new wavefront arising in the middle of the mapping area that could not be explained by propagation of a wavefront in the epicardial plane.[13] Local conduction velocity (CV) was calculated from LATs of adjacent electrodes (longitudinal, transversal, and diagonal) using discrete velocity vectors, as previously described.[14] Consistent with previous mapping studies, local conduction delay and conduction block (CB) were defined as interelectrode conduction times of 7–11 ms and ≥12 ms, respectively. Total activation time (TAT) was calculated as the time difference between the earliest and latest activated electrode.

Owing to the small size of the hearts of pediatric patients, the electrode size can be larger than the size of the heart. Therefore, TAT was corrected (cTAT) by using TAT divided by the length of the array covering BB.

An LAT, potential voltage, and fractionation distribution map of BB obtained from a 17-year-old boy with aortic valve stenosis is presented in Figure 1C.

Statistical analysis

Normally distributed continuous data are presented as mean ± standard deviation, and skewed data as median (range). Categorical data are described as numbers and percentages. Data among the 3 regions of BB were compared using the Kruskal-Wallis H test. Comparisons between patients with and without CB were made by Student *t* test, Mann–Whitney U test, $\chi 2$, or Fisher exact test when appropriate. Spearman's rank correlation was performed to evaluate the relationships between

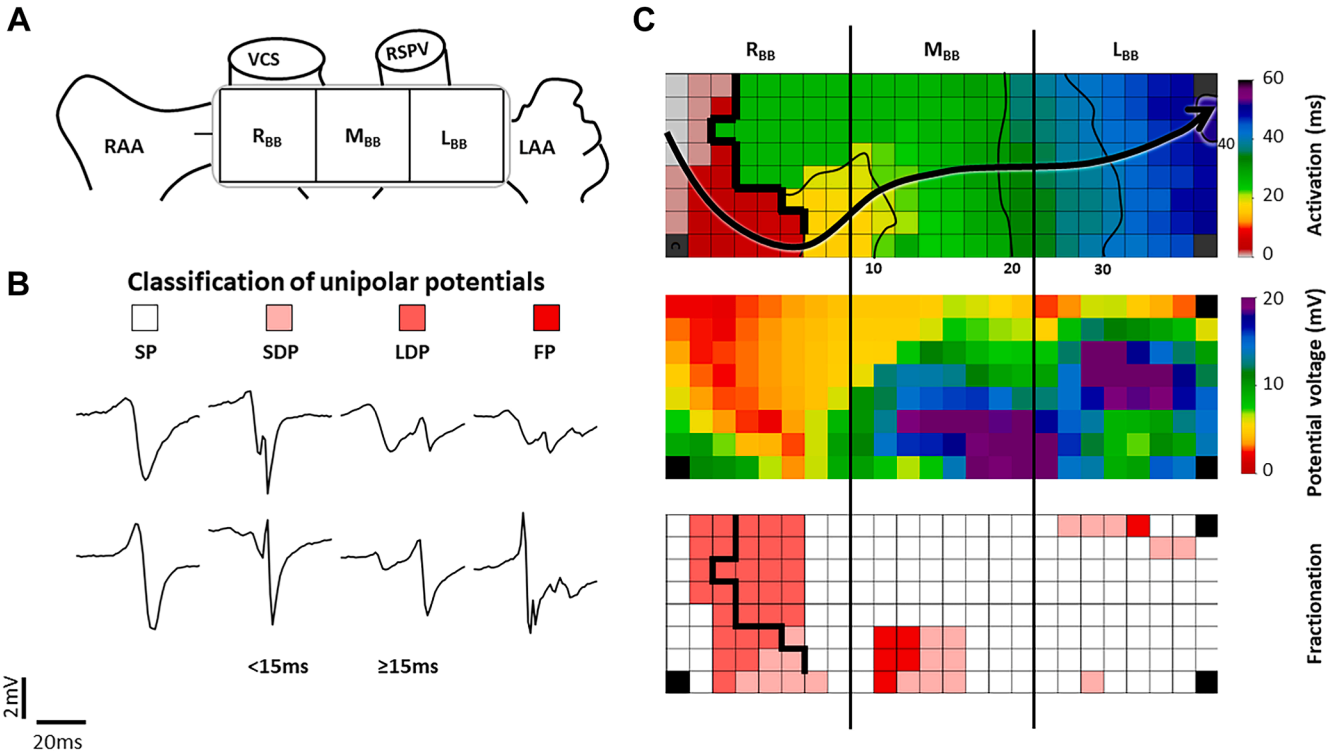

Figure 1
Mapping of BB. **A:** schematic representation of the electrode array on BB, which was divided into the right, middle, and left parts of BB. **B:** Classification of unipolar potentials. **C:** Example of local activation time map and corresponding potential voltage and fractionation maps. BB = Bachmann's Bundle; FP = fractionated potential; LAA = left atrial appendage; L_{BB} = left part of BB; LDP = long-double potential; M_{BB} = middle part of BB; RAA = right atrial appendage; R_{BB} = right part of BB; RSPV = right superior pulmonary vein; SDP = short-double potential; SP = single potential; VCS = vena cava superior.

electrophysiological parameters and (1) patient age and (2) P-wave duration. Statistical significance was defined as $P < .05$. In case of multiple testing, a Bonferroni correction was applied.

Results

Patient characteristics

A total of 55 pediatric patients (34 male [62%], age 3.2 years [0.2–17.5]) were included (Table 1), with a body mass index of 15.4 kg/m^2 (12.4–26.2). Most patients (64%) were younger than 5 years old (Supplemental Figure 1). Patients had an atrial septal defect type II (ASD II) (n = 13, 23.6%), both ventricular septal defect (VSD) and ASD II (n = 9, 16.4%), atrioventricular septal defect (n = 5, 9.1%), isolated VSD (n = 7, 12.7%), and aortic valve disease (n = 11, 20.0%). The remaining 10 patients (18.2%) were diagnosed as having various types of CHD, including partial anomalous pulmonary venous return (n = 3), tetralogy of Fallot (n = 3), Marfan syndrome (n = 1), situs inversus totalis (n = 1), aneurysm of the aorta (n = 1), and anomalous left coronary artery from the pulmonary artery (n = 1). LA and RA dilations were present in 16 patients (LA 53.3%, RA 48.5%).

Patterns of activation

LAT maps and corresponding potential voltage and fractionation maps obtained from 4 patients of different ages are

Table 1 Baseline characteristics

Baseline characteristics	
Patients	55
Male	34 (61.8)
Age, y	3.2 (0.2–17.5)
Weight, kg	14.8 (3.6–89.2)
Length, cm	100.5 (50.0–188.3)
BMI, kg/m^2	15.4 (12.4–26.2)
BSA,	0.6 (0.2–2.2)
P-wave duration, ms	0.08 ± 0.01
CHD	
ASD II	13 (23.6)
ASD II + VSD	9 (16.4)
AVSD	5 (9.1)
VSD	7 (12.7)
Aortic valve disease	11 (20)
Others*	10 (18.2)
LA dilation†	16 (16/30 = 53.3)
RA dilation‡	16 (16/33 = 48.5)

ASD = atrial septal defect; AVSD = atrioventricular septal defect; BMI = body mass index; BSA = body surface area; CHD = congenital heart disease; LA = left atrium; RA = right atrium; VSD = ventricular septal defect.
*Partial anomalous pulmonary venous return (n = 3), tetralogy of Fallot (n = 3), Marfan syndrome (n = 1), situs inversus totalis (n = 1), aneurysm of the aorta (n = 1), and anomalous left coronary artery from the pulmonary artery (n = 1)
†25 patients' data unavailable.
‡22 patients' data unavailable.

presented in Figure 2. In most patients (n = 53, 96.4%), BB was activated by a single wavefront propagating from the right to the left, as demonstrated in Figure 2A and 2B. Maps obtained from a 4.7-year-old patient with a VSD and ASD II are presented in Figure 2A. An SR wavefront smoothly propagates from the RA to the LA with a TAT of 31 ms (cTAT 1.0 ms/mm). Most potentials were SPs (89.2%) and had voltages larger than 1.0 mV (98.3%). Maps obtained from the patient with the longest TAT (54 ms, cTAT 1.7 ms/mm), which were derived from a 6.4-year-old patient with aortic valve insufficiency, are demonstrated in Figure 2B. TAT prolongation in this young patient was caused by the presence of a 17 mm long CB line at the L_{BB}. FPs were recorded from the area around the CB line, although most potentials were SPs (99.2%).

Examples of 2 complex patterns of activation are demonstrated in Figure 2C and 2D. In a 1.3-year-old patient with situs inversus totalis (Figure 2C), BB was activated by different parts of the SR wavefront separated by multiple lines of CB. The wavefronts entered BB via (opposite) multiple sites, resulting in a TAT of 43 ms (cTAT 1.3 ms/mm). A large LVA was found at the M_{BB}, together with many SDPs, LDPs, and FPs. A breakthrough wave at BB was found in only 1 patient who was diagnosed as having Loeys-Dietz syndrome and underwent a T-David procedure. As shown in Figure 2D, the breakthrough wave emerged in the M_{BB} resulting in a TAT of 25 ms (cTAT 0.8 ms/mm). Expansion of the breakthrough wave was hampered by the presence of a CB line in the right part of the mapping area, which was surrounded by LVAs, LDPs, and FPs. These 4 examples clearly show interindividual variation in the complexity of patterns of activation and potential morphology, irrespective of age.

Morphology of BB potentials

A total of 41,730 potentials (759 ± 333/patient) were recorded at BB, which, as expected, increased with age ($r = 0.787$, $P < .001$). The relative frequency distribution histogram of all unipolar potential voltages, ranging from 0.3 to 43.9 mV (median 7.1 mV), is presented in Figure 3A. From all potentials, only 3.3% of the potential voltages were smaller than 1.0 mV. In the entire population, median BB potential voltage ranged from 1.5 to 13.3 mV and was on average 7.2 ± 3.0 mV. As shown in Figure 3B, median potential voltage shows a weak, gradual increase with age ($r = 0.312$, $P = .020$). Typical examples of BB voltage maps obtained from 3 patients of different ages are shown in Figure 3D.

LVAs were observed in both the youngest (0.2 years) and oldest patients (16.8 years) but not in the patient aged 4.7

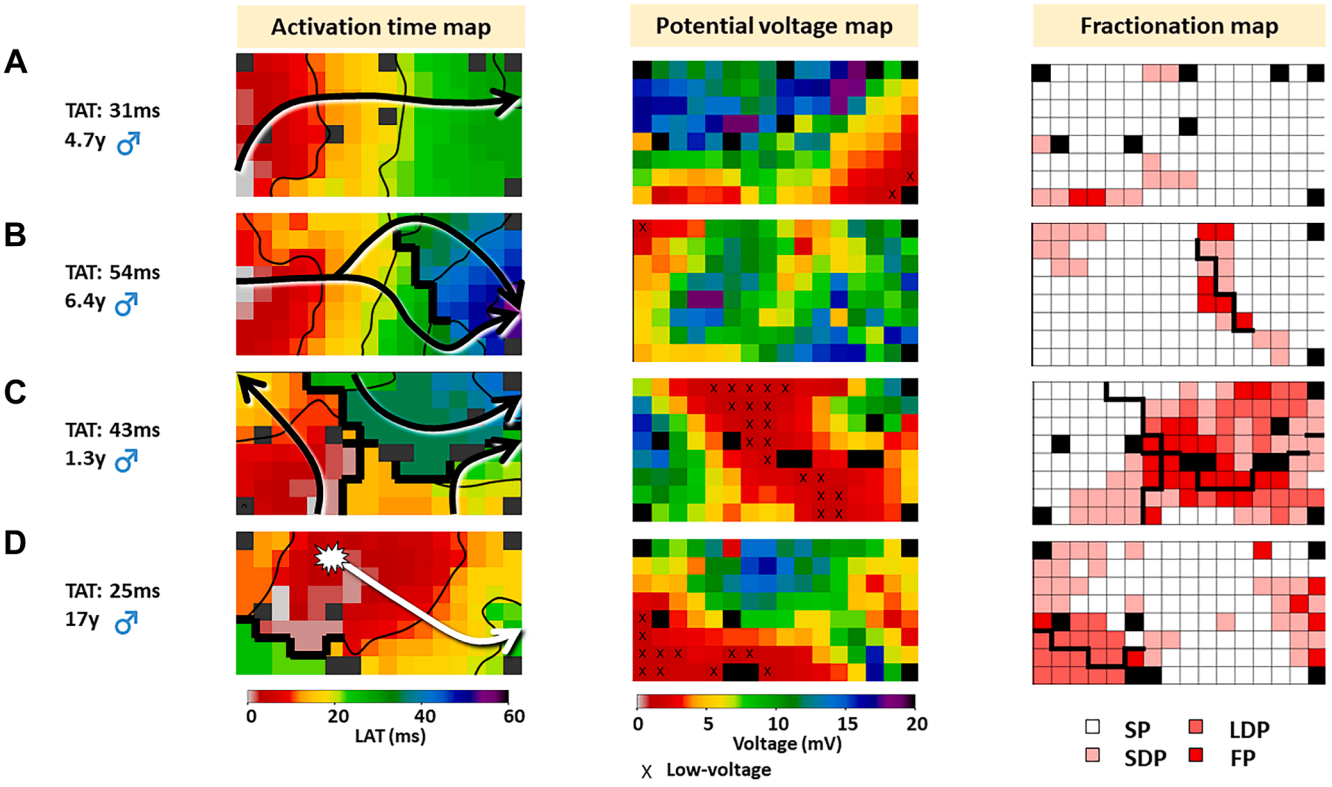

Figure 2
Mapping of Bachmann's bundle in patients of various ages. **A:** A 4.7-year-old patient in whom a typical SR wavefront propagates from the RA to the LA. **B:** A 6.4-year-old patient with the longest TAT (54 ms, cTAT 1.7 ms/mm). **C:** A 1.3-year-old patient in whom wavefronts entered BB via (opposite) multiple sites. **D:** A 17-year-old patient in whom a breakthrough wave emerged in the middle part of the BB. cTAT = corrected TAT; FP = fractionated potential; LA = left atrium; LAT = local activation time; LDP = long-double potential; LVA = low-voltage area; RA = right atrium; SDP = short-double potential; SP = single potential; SR = sinus rhythm; TAT = total activation time.

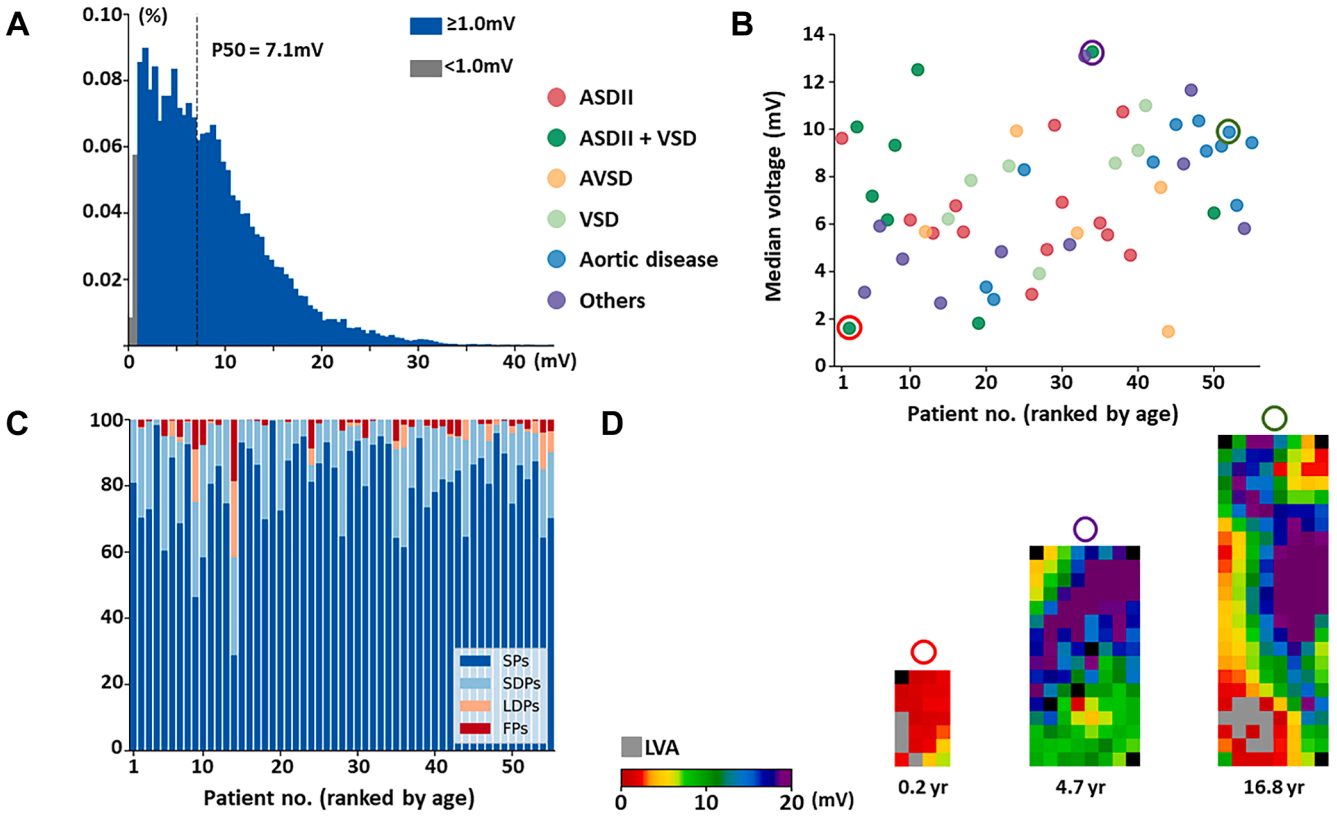

Figure 3
Bachmann's bundle unipolar potential morphologies. **A:** Relative frequency distribution histogram of all potential voltages. **B:** Plot demonstrating median potential voltage for each patient; patients are ranked by age. **C:** Stacked bar chart of different potential types for each patient; patients are ranked by age. **D:** Voltage maps obtained from 3 patients of variable ages. ASD = atrial septal defect; AVSD = atrioventricular septal defect; FP = fractionated potential; LDP = long-double potential; LVA = low-voltage area; SDP = short-double potential; SP = single potential; VSD = ventricular septal defect.

years. LVAs were found in 47 patients (85.4%), and the proportion of LVAs ranged from 0.1% to 28.6% (median 2%); there was no correlation between age and the amount of LVAs (r = −0.223, *P* = .101). The proportion of the different types of potential morphologies for each patient is presented separately in Figure 3C. In all patients, most potentials consisted of SPs (81.9% [28.8%–99.6%]). Although SDPs occurred in all patients (range: 0.4%–34.6%), LDPs occurred in 27 patients (49.1%) (range 0.1%–23.0%) and FPs in 40 patients (72.7%), ranging from 0.1% to 18.6%. There was no correlation between age and the proportion of SPs (r = 0.059, *P* = .666), SDPs (r = −0.095, *P* = .489), LDPs (r = 0.256, *P* = .059), or FPs (r = 0.109, *P* = .427).

Conduction disorders

The median local CV plotted for each patient is presented in Figure 4A; median local CV ranged from 72.9 to 121.0 cm/s and was on average 96.6 ± 10.5 cm/s. Local CV only moderately increased with age (r = 0.439, *P* < .001). The relative frequency distribution histogram of all CTs in Figure 4B shows that the prevalence of conduction delay and CB in the entire study population was 2.6% and 1.4%, respectively. CB occurred in 31 patients (56.4%), yet the proportion of CB was low (1.4% [0.1%–12.9%]). In addition, the median length of CB lines was small (3 mm [2–19]). The median longest CB length was 6 mm, and the largest CB length measured in the entire population was 38 mm. The scatter plot in Figure 4C illustrates that there is no relationship between the amount of CB and age (r = 0.109, *P* = .429). Examples of LAT maps obtained from 3 different patients with variable prevalences of CB are displayed in Figure 4D. In the 4.5-year-old patient, CB did not occur, whereas a CB line of 15 mm resulted in 3.1% CB in a 6.4-year-old and an even longer CB line of 28 mm in 14.4% CB in a patient of only 0.4 years old.

Differences between patients with and without CB are presented in Supplemental Table 2; patients with CB had less SPs (78.1% [28.8%–95.9%] vs 86.6% [60.4%–99.6%], *P* = .005) and more LDPs (0.9% [0.0%–23.0%] vs 0.0% [0.0%–1.3%], *P* < .001) and FPs (1.7% [0.0%–18.6%] vs 0.2% [0.0%–5.6%], *P* = .002). There was no difference in potential voltage, the amount of LVAs, or local CV between the 2 groups.

Of 55 patients, 4 (7.3%) had morphologic abnormalities in P wave in lead II. Patients 1 and 2, both with a VSD, had notched P waves, whereas CB was found only in patient 1 during high-resolution mapping. Patients 3 and 4 had biphasic P waves, but CB did not occur (Supplemental Figure 2). P-wave duration did not correlate with any of the

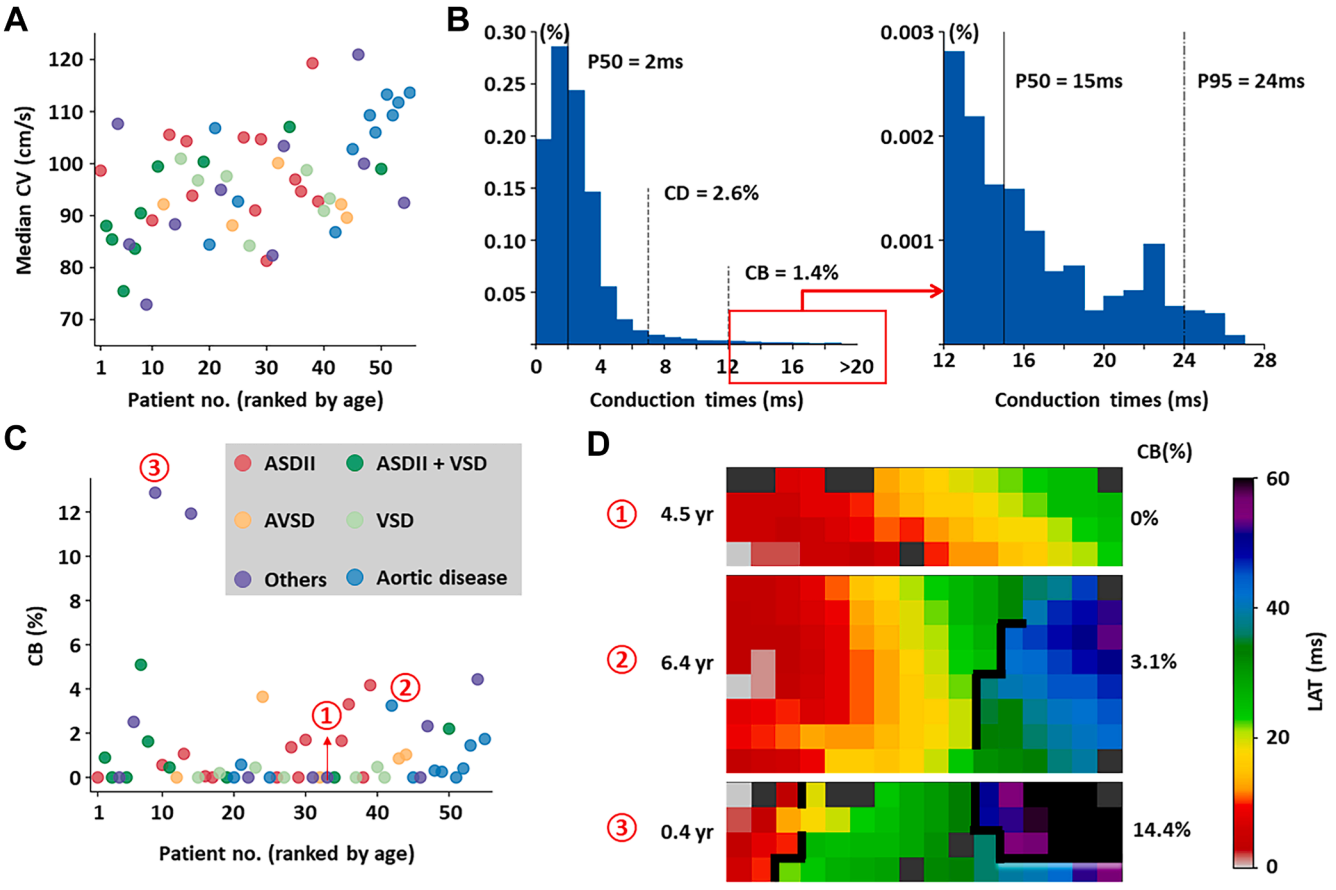

Figure 4
Conduction disorders at Bachmann's bundle. **A:** Median local conduction velocities plotted for each patient; patients are ranked by age. **B:** Relative frequency distribution histogram of all conduction times. **C:** The amount of CB plotted for each patient and 3 activation maps obtained from 3 patients of variable ages. CB = conduction block; CD = conduction delay; CV = conduction velocity; LAT = local activation time.

electrophysiological parameters after adjusting for age (Supplemental Table 3).

Regional differences in potential morphology

On average, the number of potentials recorded from the R_{BB}, M_{BB}, and L_{BB} was 250 ± 113, 267 ± 117, and 242 ± 113 (P = .511), respectively. Differences in electrophysiological parameters measured at these 3 different sites are presented in Supplemental Table 4. From the R_{BB} to the L_{BB}, the percentage of SPs gradually increased, whereas the percentage of SDPs gradually decreased. Compared with L_{BB}, R_{BB} contained more SDPs (14.4% [0.0%–84.6%] vs 6.9% [0.0–55.2%], P = .006). There were no significant differences in potential voltages or amount of LVAs among the different parts of BB.

Discussion

Key findings

Intraoperative epicardial mapping in our cohort revealed conduction abnormalities, LVAs, and abnormal potential morphology at BB in most individuals. The early electrophysiological alterations are not related to age and do not differ among the R_{BB}, L_{BB}, and M_{BB}. In addition, CV and median voltage showed age-related variation.

Conduction properties

Mapping data obtained from pediatric patients with CHD can of course not be directly compared with pediatric patients with normal hearts because the latter group does not undergo cardiac surgery. However, we can compare the outcomes of this study with mapping data obtained from adult patients with coronary artery disease. Mapping of BB in 172 patients (65 ± 9 years) without history of atrial tachyarrhythmias showed that the mean effective CV at BB was only 89 cm/s and was not dependent on age.[7] In our pediatric population, we measured a CV of 97 ± 11 cm/s, which was moderately related to age and slightly higher than adult patients. These findings indicate that the conduction in BB in adults might be affected by structural remodeling related to underlying cardiovascular diseases and aging, which differs from the cardiac maturation process in pediatric patients.

In our population, conduction disorders were already present early in childhood; CB occurred in a considerable number of patients (56.4%). These CB areas were small (on average 3 mm) but could be as long as 38 mm. Previous

mapping studies in adult patients with CHD demonstrated that conduction disorders during SR were most pronounced in the RA (particularly the intercaval region), but also BB.[2] Compared with our population, these patients had more CB (2.1% vs 1.1%) at BB, with longer CB lines, which might be explained by the longer duration of atrial volume overload and older age.

The early presence of CB at BB in our cohort is likely attributable to the underlying CHD. In a cohort of 185 adult patients (66 ± 9 years) with coronary heart disease and multiple comorbidities, CB at BB was absent in 25% of them.[7] In addition, in 25 patients with Wolff-Parkinson-White syndrome (32 ± 11 years) with normal left ventricular function and nondilated atria, high-density mapping did not reveal any CB in the RA.[15,16]

Although only 7.4% of patients had abnormal P-wave morphology on surface ECG, CB was observed in 56.4% of patients during epicardial BB mapping. Moreover, there was no correlation between P-wave duration and electrophysiological parameters. Similar results were observed in adult patients.[17–19] In small structures such as BB, conduction abnormalities may locally prolong the activation time considerably, whereas another part of the SR wavefront smoothly propagates around this area resulting in normal atrial TAT. These findings highlight the limited sensitivity of surface ECG in detecting localized atrial conduction abnormalities in pediatric BB.

Regional differences in BB electrophysiology

The R_{BB}, L_{BB}, and M_{BB} differ on both macroscopic and microscopic scales. Macroscopically, apart from the bifurcations on the left and right sides, the body of BB across the interatrial groove is broader than its thinner distal extensions.[20–22] Microscopically, although BB fibers are well aligned, the fiber orientation varies considerably from a perpendicular orientation at the junction with the superior caval vein to a more random orientation at the level of the interatrial septum (IAS).[23] Therefore, we investigated whether there were regional differences in electrophysiological properties at BB during SR. However, despite regional differences in thickness and fiber orientation, nearly all electrophysiological properties along BB were comparable, except for the prevalence of SDPs at the R_{BB}. This part of BB is formed by the fusion of muscular bands originating from the sinoatrial node and RA lateral wall, giving rise to wavefronts colliding from different bundles and multiple layers, generating SDPs.[16,20]

Patterns of activation

Most patients of our population (96.4%) showed right-to-left activation of BB, and activation emerging in the M_{BB} occurred in only 1 patient. In adult patients, right-to-left activation of BB occurred less frequently (67%), and activation wavefronts emerged from the center of BB more frequently (~12%).[6,8] A midentry site also occurs more frequently in patients with AF than those without AF.[8] It is likely that, with aging, BB fibers are damaged and cause long lines of CB. Areas behind CB may be activated by wavefronts emerging from the IAS, given that connections between BB and the IAS have been demonstrated.[20,24] In pediatric patients, BB fibers are still intact accounting for the predominant right-to-left activation of BB. One of the older patients had a midentry site, supporting the hypothesis that aging-associated remodeling of BB results in the emergence of SR wavefronts in the M_{BB}. Long-term follow-up of the pediatric patients will show whether the child with the midentry site develops atrial tachyarrhythmias at a relatively young age.

However, it is important to note that the existing data on adult BB activation patterns have so far been derived from individuals without CHD.[6,8] To date, no studies have specifically investigated BB activation patterns in adult patients with CHD. Given the structural and electrophysiological differences between CHD and non-CHD hearts and between pediatric and adult populations, our findings should not be directly extrapolated to adults with CHD.

Age, CV, and potential voltages

In the neonatal RA volume overload mouse model, volume overload diminished regularity and length of sarcomeres, expression of connexin 43, T-element density, and integrity of t-tubules of the cardiomyocytes.[25] Consequently, the calcium-handling capacity of cardiomyocytes decreased. Hence, volume overload affects the structure and function of cardiomyocytes. Dolber and Spach[26] investigated CV across BB in neonatal (1–21 days old) and adult dogs and found that longitudinal CV (131 vs 80 cm/s) in adult dogs was higher, whereas transverse CV was comparable (20 vs 19 cm/s). The higher longitudinal CV in adult dogs was attributed to a larger cardiomyocyte diameter.[26] Likewise, CV in our pediatric population also increased with age, although there was only a moderate correlation. This could be attributed to the transition from cardiomyocyte hyperplasia to hypertrophy,[11] reflecting cardiac maturation. However, after reaching adulthood, CV at BB decreases with aging.[4]

As mentioned earlier, most electrophysiological parameters did not correlate with age, suggesting that they may be influenced by additional factors beyond cardiac maturation, such as overload, inflammation, or arrhythmias.[27–30] In addition to remodeling resulting from hemodynamic abnormalities, intrinsic structural variations associated with different CHD subtypes may affect BB electrophysiology in distinct ways. For instance, more severe forms of CHD, such as situs inversus, can lead to significant conduction abnormalities and complex activation patterns at a younger age. Therefore, large patient cohorts of the various CHD subtypes are required to investigate the impact of specific CHD subtypes on BB electrophysiology.

Study limitations

Owing to the invasive nature of the mapping procedure, comparison with healthy children was not possible. Therefore, we could not establish a true "baseline" for

electrophysiological properties in pediatric BB, limiting our ability to determine whether the observed electrophysiological alterations are specific to CHD. Although previous adult studies without structural heart disease may provide a reference, they most likely do not have (normal) pediatric conduction and therefore cannot replace a healthy control group.

BB mapping was not feasible in many younger patients with CHD or those with complex CHD owing to limited surgical exposure or the unavailability of appropriate electrodes, especially in the early stages of the study. Therefore, we included only 55 patients. These exclusions were driven by technical and procedural factors, instead of selective inclusion.

Given the heterogeneity of the CHD population of the study population, relationships among electrophysiology, CHD type, and echocardiography measures could not be determined. Considerably expanding the sample size of the different CHD subtypes will help better elucidate the relationship between specific CHD and electrophysiological changes at BB.

Other atrial regions were not mapped, given that this study was focused on BB.

Conclusion

In pediatric patients with CHD, BB already contains a considerable amount of conduction disorders, LVAs, and potentials with complex morphology. The prevalence of these early electrophysiological alterations is not age related and does not differ among the R_{BB}, L_{BB}, and M_{BB}.

Funding Sources: N.M.S. de Groot, MD, PhD, is supported by funding grants from NWO-Vidi (grant number 91717339), Medical Delta, and CIRCULAR NWO (NWA.1389.20.157).

Disclosures: The authors have no conflicts of interest to disclose.

Data Availability: The data underlying this article will be shared upon reasonable request to the corresponding author.

Appendix

Supplementary data

Supplementary data associated with this article can be found in the online version at https://doi.org/10.1016/j.hrthm.2025.06.049

Address reprint requests and correspondence: Dr Natasja M.S. de Groot, Unit Translational Electrophysiology, Department of Cardiology, Erasmus Medical Center, Dr. Molewaterplein 40, 3015GD, Rotterdam, The Netherlands. E-mail address: n.m.s.degroot@erasmusmc.nl

References

1. Mouws EMJP, Lanters EAH, Teuwen CP, et al. Impact of ischemic and valvular heart disease on atrial excitation: a high-resolution epicardial mapping study. J Am Heart Assoc 2018;7:e008331.
2. Houck CA, Lanters EAH, Heida A, et al. Distribution of conduction disorders in patients with congenital heart disease and right atrial volume overload. JACC Clin Electrophysiol 2020;6:537–548.
3. Kharbanda RK, van Schie MS, Ramdat Misier NL, et al. First evidence of atrial conduction disorders in pediatric patients with congenital heart disease. JACC Clin Electrophysiol 2020;6:1739–1743.
4. Van Der Does WFB, Houck CA, Heida A, et al. Atrial electrophysiological characteristics of aging. J Cardiovasc Electrophysiol 2021;32:903–912.
5. Schram-Serban C, Heida A, Roos-Serote MC, et al. Heterogeneity in conduction underlies obesity-related atrial fibrillation vulnerability. Circ Arrhythm Electrophysiol 2020;13:e008161.
6. van Schie MS, Veen D, Kharbanda RK, et al. Characterization of pre-existing arrhythmogenic substrate associated with de novo early and late postoperative atrial fibrillation. Int J Cardiol 2022;363:71–79.
7. Teuwen CP, Yaksh A, Lanters EAH, et al. Relevance of conduction disorders in Bachmann's bundle during sinus rhythm in humans. Circ Arrhythm Electrophysiol 2016;9:e003972.
8. Heida A, van Schie MS, van der Does WFB, Taverne YJHJ, Bogers AJJC, De Groot NMS. Reduction of conduction velocity in patients with atrial fibrillation. J Clin Med 2021;10:2614.
9. Teuwen CP, van der Does LJME, Kik C, et al. Sinus rhythm conduction properties across Bachmann's bundle: impact of underlying heart disease and atrial fibrillation. J Clin Med 2020;9:1875.
10. Teuwen CP, Ramdjan TTTK, Götte M, et al. Time course of atrial fibrillation in patients with congenital heart defects. Circ Arrhythm Electrophysiol 2015;8:1065–1072.
11. Salameh S, Ogueri V, Posnack NG. Adapting to a new environment: postnatal maturation of the human cardiomyocyte. J Physiol 2023;601:2593–2619.
12. van Schie MS, Starreveld R, Bogers AJJC, de Groot NMS. Sinus rhythm voltage fingerprinting in patients with mitral valve disease using a high-density epicardial mapping approach. Europace 2021;23:469–478.
13. Mouws EMJP, Lanters EAH, Teuwen CP, et al. Epicardial breakthrough waves during sinus rhythm. Circ Arrhythm Electrophysiol 2017;10:e005145.
14. van Schie MS, Heida A, Taverne YJHJ, Bogers AJJC, de Groot NMS. Identification of local atrial conduction heterogeneities using high-density conduction velocity estimation. Europace 2021;23:1815–1825.
15. Konings KT, Kirchhof CJ, Smeets JR, Wellens HJ, Penn OC, Allessie MA. High-density mapping of electrically induced atrial fibrillation in humans. Circulation 1994;89:1665–1680.
16. Konings KTS, Smeets JLRM, Penn OC, Wellens HJJ, Allessie MA. Configuration of unipolar atrial electrograms during electrically induced atrial fibrillation in humans. Circulation 1997;95:1231–1241.
17. van der Does WFB, Heida A, van der Does LJME, Bogers AJJC, de Groot NMS. Conduction disorders during sinus rhythm in relation to atrial fibrillation persistence. J Clin Med 2021;10:2846.
18. Teuwen CP, Kik C, van der Does LJME, et al. Quantification of the arrhythmogenic effects of spontaneous atrial extrasystole using high-resolution epicardial mapping. Circ, Arrhythm Electrophysiol 2018;11:e005745.
19. Ramdat Misier NL, van Schie MS, Li C, et al. Epicardial high-resolution mapping of advanced interatrial block: relating ECG, conduction abnormalities and excitation patterns. Front Cardiovasc Med 2022;9:1031365.
20. Knol WG, Teuwen CP, Kleinrensink GJ, Bogers AJJC, De Groot NMS, Taverne YJHJ. The Bachmann bundle and interatrial conduction: comparing atrial morphology to electrical activity. Heart Rhythm 2019;16:606–614.
21. Khaja A, Flaker G. Bachmann's bundle: does it play a role in atrial fibrillation? Pacing Clin Electrophysiol 2005;28:855–863.
22. Lemery R, Guiraudon G, Veinot JP. Anatomic description of Bachmann's bundle and its relation to the atrial septum. Am J Cardiol 2003;91:1482–1485.
23. van Campenhout MJH, Yaksh A, Kik C, et al. Bachmann's bundle: a key player in the development of atrial fibrillation? Circ Arrhythm Electrophysiol 2013;6:1041–1046.
24. van Schie MS, Ramdat Misier NL, Knops P, Heida A, Taverne YJHJ, de Groot NMS. Mapping-guided atrial lead placement determines optimal conduction across Bachmann's bundle: a rationale for patient-tailored pacing therapy. Europace 2023;25:1432–1440.
25. Dong Z, Chen D, Zheng S, et al. Volume overload impedes the maturation of sarcomeres and T-tubules in the right atria: a potential cause of atrial arrhythmia following delayed atrial septal defect closure. Front Physiol 2023;14:1237187.
26. Dolber PC, Spach MS. Structure of canine Bachmann's bundle related to propagation of excitation. Am J Physiol 1989;257:H1446–H1457.
27. Mitrofanova LB, Orshanskaya V, Ho SY, Platonov PG. Histological evidence of inflammatory reaction associated with fibrosis in the atrial and ventricular walls in a case-control study of patients with history of atrial fibrillation. Europace 2016;18(suppl 4):iv156–iv162.
28. Platonov PG, Mitrofanova LB, Orshanskaya V, Ho SY. Structural abnormalities in atrial walls are associated with presence and persistency of atrial fibrillation but not with age. J Am Coll Cardiol 2011;58:2225–2232.
29. Ueda A, Adachi I, McCarthy KP, Li W, Ho SY, Uemura H. Substrates of atrial arrhythmias: histological insights from patients with congenital heart disease. Int J Cardiol 2013;168:2481–2486.
30. Broberg CS, Chugh SS, Conklin C, Sahn DJ, Jerosch-Herold M. Quantification of diffuse myocardial fibrosis and its association with myocardial dysfunction in congenital heart disease. Circ, Cardiovasc Imaging 2010;3:727–734.